ANTIOXIDANTS & REDOX SIGNALING
Volume 17, Number 11, 2012

DOI: 10.1089/ars.2011.4312

Redox Proteomics Analyses of the Influence of Co-Expression of Wild-Type or Mutated LRRK2 and Tau on *C. elegans* Protein Expression and Oxidative Modification: Relevance to Parkinson Disease

Fabio Di Domenico,[1,2] Rukhsana Sultana,[1] Andrew Ferree,[3] Katelyn Smith,[3] Eugenio Barone,[1,4] Marzia Perluigi,[2] Raffaella Coccia,[2] William Pierce,[5] Jian Cai,[5] Cesare Mancuso,[4] Rachel Squillace,[6] Manfred Wiengele,[6] Isabella Dalle-Donne,[7] Benjamin Wolozin,[3,8] and D. Allan Butterfield[2]

Abstract

Aims: The human LRRK2 gene has been identified as the most common causative gene of autosomal-dominantly inherited and idiopathic Parkinson disease (PD). The G2019S substitution is the most common mutation in LRRK2. The R1441C mutation also occurs in cases of familial PD, but is not as prevalent. Some cases of LRRK2-based PD exhibit Tau pathology, which suggests that alterations on LRRK2 activity affect the pathophysiology of Tau. To investigate how LRRK2 might affect Tau and the pathophysiology of PD, we generated lines of *C. elegans* expressing human LRRK2 [wild-type (WT) or mutated (G2019S or R1441C)] with and without V337M Tau. Expression and redox proteomics were used to identify the effects of LRRK2 (WT and mutant) on protein expression and oxidative modifications. ***Results:*** Co-expression of WT LRRK2 and Tau led to increased expression of numerous proteins, including several 60S ribosomal proteins, mitochondrial proteins, and the V-type proton ATPase, which is associated with autophagy. *C. elegans* expressing mutant LRRK2 showed similar changes, but also showed increased protein oxidation and lipid peroxidation, the latter indexed as increased protein-bound 4-hydroxy-2-nonenal (HNE). ***Innovation:*** Our study brings new knowledge about the possible alterations induced by LRRK2 (WT and mutated) and Tau interactions, suggesting the involvement of G2019S and R1441C in Tau-dependent neurodegenerative processes. ***Conclusion:*** These results suggest that changes in LRRK2 expression or activity lead to corresponding changes in mitochondrial function, autophagy, and protein translation. These findings are discussed with reference to the pathophysiology of PD. *Antioxid. Redox Signal.* 17, 1490–1506.

Introduction

Parkinson disease (PD) is the second most prevalent degenerative disease of the nervous system. Functional studies of PD-related genes implicate dysfunction of mitochondria, autophagy, and the stress response in the pathophysiology of PD (11, 42, 47).

At least nine different genes are known to cause familial PD. Mutations in the α-synuclein, parkin, microtubule associated protein tau (MAPT), ubiquitin carboxy-terminal hydrolase L1 (UCH-L1), DJ-1, PTEN-induced kinase 1 (PINK1), and leucine-rich repeat kinase 2 (LRRK2) genes have been implicated in hereditary PD (16, 19).

The LRRK2 gene has been identified as the most common causative gene of autosomal-dominant inherited and idiopathic PD (54). The LRRK2 gene encodes a complex multidomain protein (2527 amino acids; 286 kDa,). The LRRK2 gene has specific domains including N-terminal ankyrin

[1]Department of Chemistry, Center of Membrane Sciences, and Sanders-Brown Center on Aging, University of Kentucky, Lexington, Kentucky.
[2]Department of Biochemical Sciences, Sapienza University of Rome, Rome, Italy.
[3]Department of Pharmacology, Boston University, Boston, Massachusetts.
[4]Institute of Pharmacology, Catholic University of Rome, Rome, Italy.
[5]Department of Pharmacology, University of Louisville, Louisville, Kentucky.
[6]Ariad Pharmaceuticals, Cambridge, Massachusetts.
[7]Department of Biology, University of Milan, Milan, Italy.
[8]Edith Nourse Rogers Memorial Veterans Affairs Medical Center, Bedford, Massachusetts.

Innovation

Our proteomics study is the first of its kind to identify altered expression and altered oxidatively modified proteins in transgenic *C. elegans* models associated with PD. Our study brings new knowledge on the possible alteration induced by LRRK2 (WT and mutated) and Tau interactions, identified as impaired autophagy, energy metabolism, proteasomal function, and cellular structure among others, suggesting the involvement of G2019S and R1441C in Tau-dependent neurodegenerative processes.

repeats, a leucine-rich repeat (LRR) region, a catalytic core, featuring a functional ROC (Ras Complex proteins), a GTPase domain, and a kinase domain (mitogen-activated protein kinase kinase kinase, MAPKKK) linked by the C- terminus of ROC (COR), followed by a C-terminal WD40 domain (37). *In vitro* studies demonstrated that LRRK2 is both a functional kinase and a GTPase, able to undergo autophosphorylation and perform phosphorylation of generic and putative physiological substrates (20).

Experimental evidence suggests LRRK2 may play a role in neuritic outgrowth and branching (8), and the presence of both a ROC/GTPase and a kinase domain suggests that LRRK2 plays a role in intracellular signaling. Overexpression of wild-type LRRK2 induces neuronal cell death, neurite shortening, protein aggregation, oxidative stress-induced cell death, and increased levels of intracellular reactive oxygen species (ROS) (34, 51).

LRRK2 is present in the cytoplasm but also associates with numerous organelles, such as mitochondria, endoplasmic reticulum, trans-Golgi, and also with the plasma membrane (24, 50). To date, R1441C/G, Y1699C, G2019S, and I2020T mutations have proven to be pathogenic (11, 48). The clinical symptoms of LRRK2 mutation carriers are similar to those of idiopathic PD patients, whereas the related neuropathology is pleomorphic, including α-synucleinopathy, tauopathy, and ubiquitin deposits or nigral neuronal loss solely (11, 43, 61). Among identified mutations of LRRK2, the amino acid substitution G2019S has been regarded as the most common cause of dominantly inherited as well as sporadic PD (14, 40). Previous studies showed that G2019S augments LRRK2 autophosphorylation and kinase activity, which cause neurite degeneration and neuronal cell death (34, 51, 57), suggesting a mechanism of toxic gain-of-function, probably related to deregulation of LRRK2 kinase activity. The R1441C mutation is another frequent LRRK2 mutation. This mutation decreases the GTPase activity of LRRK2 and could destabilize the interaction between monomers, which might be the mechanism of enzymatic dysfunction (28–30).

The interconnection between PD and Tau is suggested by the identification of mutations in the Tau-encoding MAPT gene that are linked to frontotemporal dementia with Parkinsonism (59). Mutations in LRRK2 generate PD that is sometimes associated with Tau pathology (19). Based on this correlation, we hypothesize that LRRK2 kinase dysfunction leads to deregulation of the post-translational state of Tau (31, 33), which in turn controls its compartmentalization and finally its functional roles in neuronal maintenance.

We previously generated lines of *Caenorhabditis. elegans* expressing human wild-type (WT) LRRK2 and the mutants, G2019S and R1441C (47). In the current study, we have crossed these lines with a line of *C. elegans* expressing V337M Tau to investigate how mutations in LRRK2 might contribute to disease. We explored these questions using expression proteomics and redox proteomics methods (13).

Results

Characterization of LRRK2 C. elegans *strains*

The crossing of nematodes expressing LRRK2 and Tau V337M produced viable offspring with no effects on lifespan or fertility but severe movement impairments. The motor deficits were quantified with the thrashing assay, as this has been shown to be a reliable indicator of Tau pathology in *C. elegans* (23, 26, 27). The combination of LRRK2 and Tau V337M produced a significant reduction in thrashing performance compared to both nontransgenic and Tau V337M alone (Fig. 1).

Total protein oxidation levels

As a starting point for the study, we measured by slot blot analysis protein oxidative modification indexed as protein carbonylation, protein-resident 3-nitrotyrosine (3NT), and protein-bound HNE. In the analysis of total protein carbonyl levels shown in Figure 2, we saw no significant difference between nontransgenic (Non-T), Tau V337M transgenic (Tau), and LRRK2::Tau transgenic samples whether we compared them using as the control group Non-T or Tau. Interestingly, the carbonyl levels of LRRK2::Tau are lower than Non-T or TAU but did not reach statistical significance.

Comparing protein-bound 3NT levels of Non-T with LRRK2::Tau samples (Fig. 2), we showed a significant increase of 133%, 130%, and 166% in WT/TAU, G2019S::Tau, and R1441C::Tau, respectively. The comparison of LRRK2::Tau transgenic samples with Tau transgenic samples in contrast showed a significant increase in protein-bound 3NT levels only for the R1441C::Tau sample.

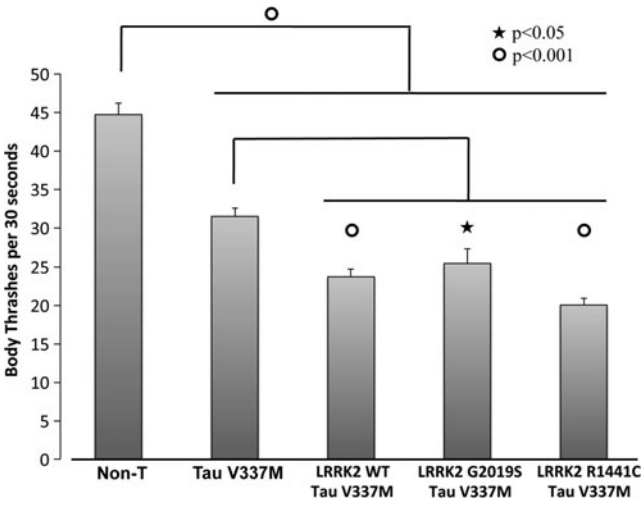

FIG. 1. Bar graph of body trashes count in 30 sec in *C. elegans* transgenic and nontransgenic strains. Raw data are reported.

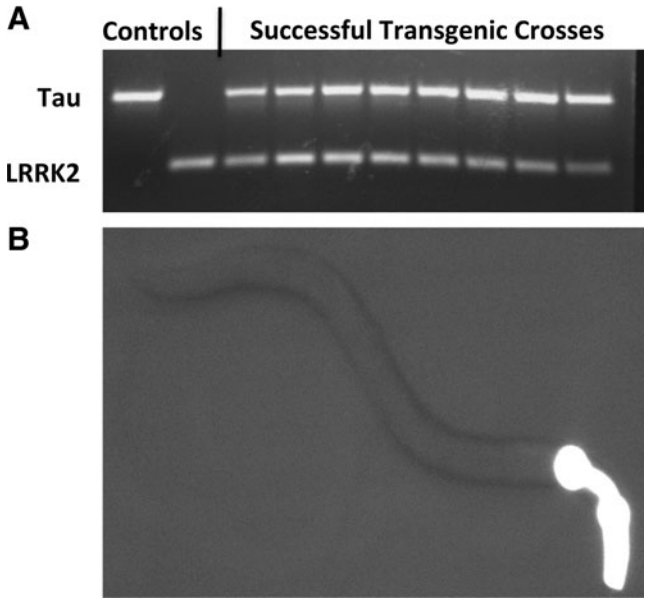

FIG. 2. (A) PCR gel of tau and LRRK2 gene expression; (B) Expression of GFP in the pharyngeal muscles of a young adult transgenic *C. elegans* expressing Tau V337M. Fluorescence was used as a preliminary indicator of transgene expression. Image taken with a 20× objective.

The last parameters of oxidative modification employed was protein-bound HNE. Figure 3 shows increased protein-bound HNE for LRRK2::Tau transgenic samples compared both with Non-T and with TAU that present nearly the same value: For the WT::Tau sample, the mean increase was 141% when compared to Non-T and 139% when compared to Tau samples; for G2019S/TAU the mean increase was 160% and 158%, and for R1441C::Tau the mean increase was 145% and 143%, respectively.

Proteomics and redox proteomics analysis

In the proteomics study, we analyzed the difference in protein expression levels, and for the redox proteomics analysis we identified proteins with altered protein-bound HNE levels. We considered for the analysis the seven groups previously described, showing first the comparison with nontransgenic samples and then with Tau transgenic samples as controls. The HNE blot values were normalized to the expression values on gels to yield specific protein-bound HNE levels per protein. The proteins with two or more percentage values listed were identified in two or more different spots. The proteomics and redox proteomics results are reported in Table 1 and shown in Figures 4, 5, and 6.

Tau vs. *nontransgenic*

In the comparison of Tau samples with Non-T we identified a significant increase in expression levels of three proteins in tau transgenic (Table 1A; Fig. 4). These proteins (with % increased values) are heat shock protein 25, isoform a (240%), 60S ribosomal protein L22 (211%), and tubulin alpha-2 chain (157%).

In the analysis of protein-bound HNE levels (Table 1A; Figs. 5 and 6), we identified for Tau samples compared with Non-T increased levels of three proteins: 40S ribosomal protein SA (347%), fructose-bisphosphate aldolase 1 (276% and 719%), and aminopeptidase (770%). We show also decreased levels of two proteins: propionyl-CoA carboxylase alpha chain mitochondrial (42%) and aspartic protease (38%).

LRRK2 WT::Tau vs. *nontransgenic*

The proteomics comparison between LRRK2 WT::Tau with Non-T samples identified increased expression levels of five proteins (Table 1B; Fig. 4): Bis(5′-nucleosyl)-tetraphosphatase (201%), protein F53F1.2 (184%), vitellogenin-6 (251%), NADH ubiquinone oxidoreductase protein 2 (327%), and myosin regulatory light chain 1 (189%); decreased expression levels of six proteins were identified: glyceraldehyde-3-phosphate dehydrogenase (60%), dihydrolipoyl dehydrogenase (45%), 60S ribosomal protein L7 (48%), histone H4 (46%), nematode polyprotein allergen related protein (37%), and actin-depolymerizing factor 2, isoform c (56%).

The analysis of protein-bound HNE levels identified increased levels in two proteins (Table 1B; Figs. 5 and 6): disorganized muscle protein 1 (846%) and transitionally controlled tumor protein (3968%); and decreased protein-bound HNE levels of two proteins: 40S ribosomal protein SA (4%) and proteasome subunit alpha type-5 (18%).

LRRK2 G2019S::Tau vs. *nontransgenic*

In the expression levels analysis between LRRK2 G2019S::Tau with Non-T samples, we identified nine proteins with increased levels (Table 1C; Fig. 4): 60S ribosomal protein L22 (731%), calponin protein 4 (171%), triosephosphate isomerase (214%, 187%), elongation factor 2 (214%), vitellogenin-6 (317%), fructose-1,6-biphosphatase protein 1 (441%), probable aconitate hydratase mitochondrial (206%), bis(5′-nucleosyl)-tetraphosphatase (191%), and heat shock protein 25, isoform a (304%); and decreased levels only for tubulin alpha-2 chain (38%).

The redox proteomics analysis identified 10 proteins with increased protein-bound HNE levels (Table 1C; Figs. 5 and 6): disorganized muscle protein 1 (305%), probable ornithine aminotransferase mitochondrial (309%), proteasome subunit beta type-2 (268%), ATP synthase subunit beta mitochondrial (388%), probable adenylate kinase isoenzyme F38B2.4 (727%), probable glutaryl-CoA dehydrogenase, mitochondrial (1222%), fatty acid binding protein 2 homologue (357%), guanine nucleotide binding protein beta 2 (587%), ZK829.4 protein (260%), and aspartic protease (256%).

LRRK2 R1441C::Tau vs. *nontransgenic*

In the expression levels analysis between LRRK2 R1441C::Tau with Non-T samples, we identified increased levels of 10 proteins (Table 1D; Fig. 4): heat shock protein 25 isoform a (352%), triosephosphate isomerase (161%, 183%), malate dehydrogenase (161%, 145%, 331%), fructose-1,6-biphosphatase protein 1 (242%), vitellogenin-6 (270%), fatty acid and retinol-binding protein 1 (210%), 60S ribosomal protein L22 (350%), calponin protein 4 (156%), protein F53F1.2 (163%), and elongation factor 2 (215%); and decreased expression levels only for histone H4 (62%).

The redox proteomics analysis of protein-bound HNE levels identified increased levels in four proteins (Table 1D;

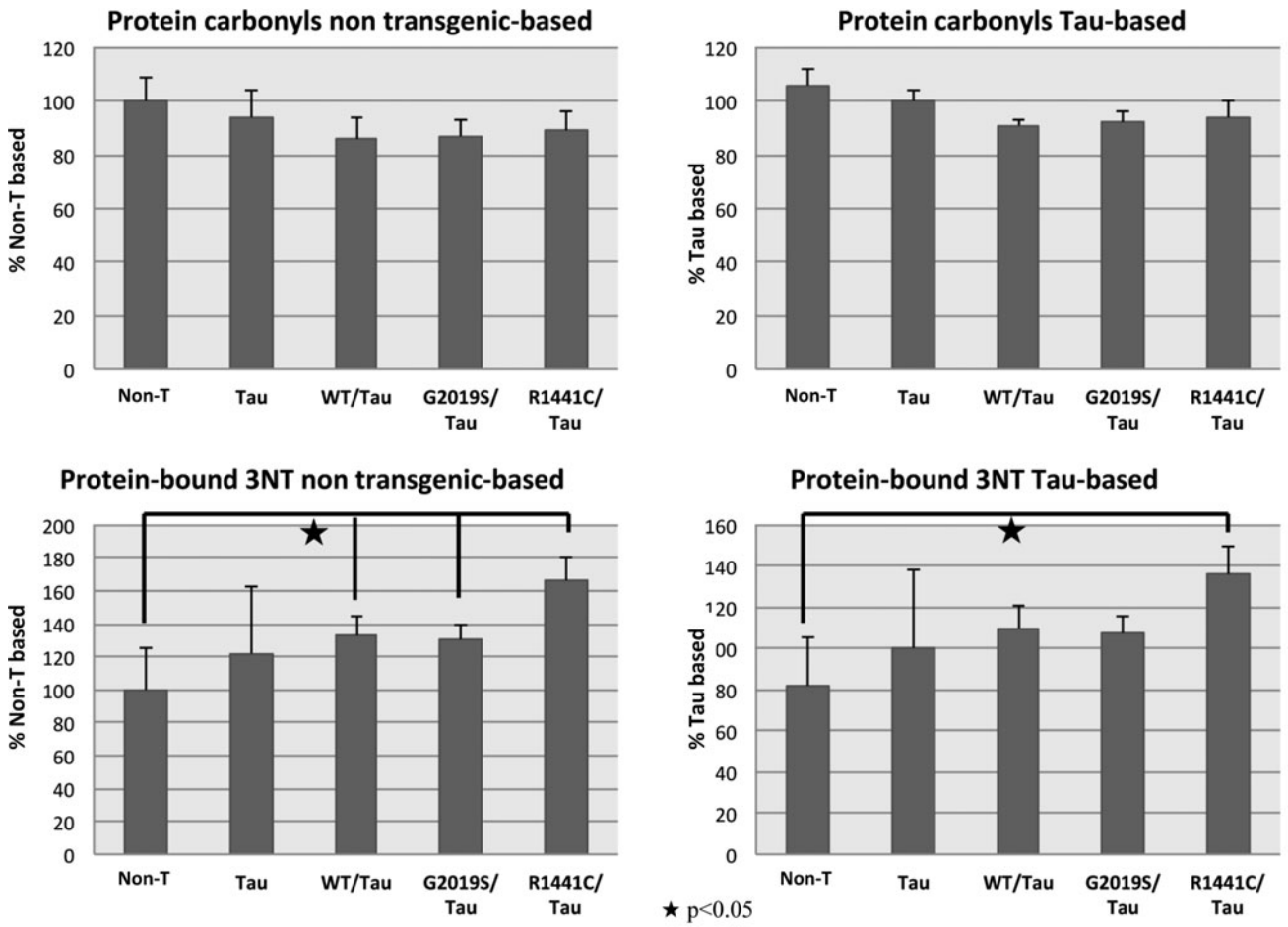

FIG. 3. Bar graph of total protein carbonyls and total protein-bound 3NT in *C. elegans* transgenic and nontransgenic strains. Each value was compared before to the nontransgenic strain and after to the Tau strain, set as 100%. The symbols represent significant differences with p value < 0.05.

Figs. 5 and 6): actin-1/3 (320%), fructose-bisphosphate aldolase 1 (984%), tubulin beta-2 chain (857%), and eukaryotic initiation factor 4A (862%); and decreased protein-bound HNE levels only for beta-galactoside-binding lectin (3%).

LRRK2 WT::Tau vs. *Tau*

The proteomics comparison between LRRK2 WT::Tau transgenic with Tau samples identified decreased expression levels for eight proteins (Table 1E, Fig. 4): elongation factor 2 (32%), histone H4 (46%), nematode polyprotein allergen related protein (40%), glyceraldehyde-3-phosphate dehydrogenase (60%), 60S ribosomal protein L7 (51%), dihydrolipoyl dehydrogenase (53%), fructose-1,6-biphosphatase protein 1 (81%), and probable aconitate hydratase mitochondrial (54%); and increased levels for five proteins: V-type proton ATPase (366%), actin-depolymerizing factor 2, isoform c (664%), triosephosphate isomerase (259%, 660%), proteasome subunit alpha type-1 (190%), and bis(5′-nucleosyl)-tetraphosphatase (167%).

The redox proteomics analysis of protein-bound HNE levels identified increased levels of four proteins (Table 1E; Figs. 5 and 6): ribosomal protein L7 (569%), disorganized muscle protein 1 (238%), heat shock 70 kDa protein F mitochondrial (296%), and beta-galactoside-binding lectin (350%).

LRRK2 G2019S::Tau vs. *Tau*

In the proteomics expression levels analysis between LRRK2 G2019S::Tau with Tau samples, we identified increased levels of four proteins (Table 1F; Fig. 4): triosephosphate isomerase (194%, 797%, 183%), V-type proton ATPase (227%), 60S ribosomal protein L22 (151%), and fructose-1,6-biphosphatase protein 1 (182%); and decreased expression levels of three proteins: protein F01G10.1 (67%), GTP-binding nuclear protein ran-1 (68%), and arginine kinase (63%).

The redox proteomics analysis of protein-bound HNE identified increased levels of 17 proteins (Table 1F; Figs. 5 and 6): heat shock 70 kDa protein F mitochondrial (308%), ribosomal protein L6 (656%), probable inorganic pyrophosphatase 1 (249%), vitellogenin-6 (929%), actin-1/3 (923%), enolase (173%, 188%), V-type proton ATPase (357%), heat shock 70 kDa protein A (191%), proteasome subunit beta type-2 (261%), eukaryotic translation initiation factor (585%), methylmalonate-semialdehyde dehydrogenase (618%), fatty acid binding protein 2 homologue (414%), probable arginine kinase (453%), guanine nucleotide binding protein beta 2 (629%), ZK829.4 protein (396%), citrate synthase mitochondrial (285%), and aminopeptidase (163%).

Table 1. Proteins Identified by Proteomics and Redox Proteomics

Table 1A

Tau vs. *Non transgenic*	*Protein name*	*Swiss prot accession number*	Pb*	*Peptides matched/ searched*	P *value*†	*Fold increase/ decrease*	*Function*
10E	Heat shock protein 25, isoform a	Q17849	1e-011	4/5	0.004	2.41 ↑	Chaperone
7E	60S ribosomal protein L22	P52819	5e-005	2/2	0.005	2.11 ↑	Protein biosynthesis
4E	Tubulin alpha-2 chain	P34690	1e-014	15/20	0.012	1.57 ↑	Cell structure
42H	40S ribosomal protein SA	P46769	6e-014	8/14	0.040	3.47 ↑	Protein biosynthesis
49H	Fructose-bisphosphate	P54216	1e-030	9/19	0.014	2.76↑	Energy metabolism
50H	aldolase 1		5e-015	6/9	0.042	7.19 ↑	
51H	Propionyl-CoA carboxylase alpha chain, mitochondria	Q612F5	1e-007	2/3	0.045	0.42 ↓	Energy metabolism
37H	Aminopeptidase	Q27245	6e-006	5/13	0.040	7.70 ↑	Protein degradation
40H	Aspartic protease	O76830	2e-009	3/7	0.026	0.38 ↓	Protein degradation

Table 1B

LRRK2 wt::Tau vs. *nontransgenic*	*Protein name*	*Swiss prot accession number*	Pb	*Peptides matched/ searched*	P *value*	*Fold increase/ decrease*	*Function*
19E	Glyceraldehyde-3-phosphate dehydrogenase	P17330	2e-009	6/48	0.004	0.60 ↓	Energy metabolism
16E	Dihydrolipoyl dehydrogenase	O17953	9e-012	4/7	0.005	0.45 ↓	Pyruvate dehydrogenase complex
25E	60S ribosomal protein L7	O01802	1e-013	2/3	0.005	0.48 ↓	Protein biosynthesis
38E	Bis(5′-nucleosyl)-tetraphosphatase	Q9U2M7	2e-009	2/2	0.008	2.01 ↑	Induction of apoptosis
2E	Histone H4	P62784	3e-006	3/3	0.011	0.46 ↓	Nucleosome structure
22E	Protein F53F1.2,	P91997	3e-013	5/8	0.024	1.84 ↑	Oxidoreductase activity
23E	NADH ubiquinone oxidoreductase protein 2,	O01602	8e-012	4/8	0.027	3.27 ↑	Energy metabolism
12E	Nematode polyprotein allergen related protein	Q86S16	2e-010	2/4	0.028	0.37 ↓	Development regulation
41E	Vitellogenin-6	P18948	2e-014	18/36	0.035	2.51 ↑	Nutrient reservoir activity
29E	Actin-depolymerizing factor 2	Q07749	8e-013	6/15	0.037	0.56 ↓	Cell structure
5E	Myosin regulatory light chain 1	P19625	4e-005	2/3	0.040	1.89 ↑	Muscle structure
3H	Disorganized muscle protein 1	Q18066	4e-015	16/35	0.015	8.96 ↑	Myofilaments structure
42H	40S ribosomal protein SA	P46769	6e-014	8/14	0.022	0.04 ↓	Protein biosynthesis
54H	Proteasome subunit alpha type-5	Q95008	2e-016	10/21	0.042	0.18 ↓	Protein degradation
39H	Translationally-controlled tumor protein	Q93573	7e-013	4/15	0.014	36.98 ↑	Microtubule stabilization

Table 1C

LRRK2 wt::Tau vs. *Tau*	*Protein name*	*Swiss prot accession number*	Pb	*Peptides matched/ searched*	P *value*	*Fold increase/ decrease*	*Function*
13E	Elongation factor 2	P29691	2e-009	7/10	0.002	0.32 ↓	Protein biosynthesis
2E	Histone H4	P62784	3e-006	3/3	0.003	0.46 ↓	Nucleosome structure
12E	Nematode polyprotein allergen related protein	Q86S16	2e-010	2/4	0.003	0.40 ↓	Development regulation
3E	V-type proton ATPase subunit A	Q9XW92	1e-012	24/45	0.011	3.66 ↑	Lysosome structure/ autophagy

(*continued*)

TABLE 1C. CONTINUED

LRRK2 wt::Tau vs. *Tau*	*Protein name*	*Swiss prot accession number*	Pb	*Peptides matched/ searched*	P *value*	*Fold increase/ decrease*	*Function*
19E	Glyceraldehyde-3-phosphate dehydrogenase	P17330	2e-009	6/48	0.012	0.60 ↓	Energy metabolism
37E	Actin-depolymerizing factor 2,	Q07749	8e-010	5/7	0.019	6.64 ↑	Cell structure
34E	Triosephosphate isomerase	Q10657	1e-010	7/17	0.022	2.59 ↑	Energy metabolism
28E			7e-011	5/7	0.004	2.56 ↑	
36E			1e-010	3/4	0.022	6.60 ↑	
25E	60S ribosomal protein L7	O01802	1e-013	2/3	0.027	0.51 ↓	Protein biosynthesis
16E	Dihydrolipoyl dehydrogenase	O17953	9e-012	4/7	0.032	0.53 ↓	
9E	Fructose-1,6-biphosphatase protein 1	Q9N2M2	6e-011	5/7	0.035	0.81 ↓	Energy metabolism
42E	Probable aconitate hydratase, mitochondrial	P34455	5e-014	13/24	0.044	0.54 ↓	Energy metabolism
33E	Proteasome subunit alpha type-1	O44156	8e-013	2/2	0.047	1.90 ↑	Protein degradation
38E	Bis (5′-nucleosyl)-tetraphosphatase	Q9U2M7	2e-009	2/2	0.040	1.67 ↑	Apoptosis induction
1H	60S ribosomal protein L7	O01802	1e-030	2/4	0.035	5.69 ↑	Protein biosynthesis
3H	Disorganized muscle protein 1	Q18066	4e-015	16/35	0.035	2.38 ↑	Myofilament structure
4H	Heat shock 70 kDa protein F, mitochondrial	P11141	5e-014	7/12	0.031	2.96 ↑	Chaperone
5H	beta-galactoside-binding lectin	P36573	1e-014	5/13	0.032	3.50 ↑	Sugar binding

TABLE 1D

LRRK2 G2019S::Tau vs. *nontransgenic*	*Protein name*	*Swiss prot accession number*	Pb	*Peptides matched/ searched*	P *value*	*Fold increase/ decrease*	*Function*
4E	Tubulin alpha-2 chain	P34690	1e-014	15/20	0.0003	0.38 ↓	Cell structure
7E	60S ribosomal protein L22	P52819	5e-005	2/2	0.0003	7.31 ↑	Protein biosynthesis
32E	Calponin protein 4,	O44727	3e-010	2/3	0.005	1.71 ↑	Muscle structure
28E	Triosephosphate	Q10657	7e-011	5/7	0.009	2.14 ↑	Energy metabolism
34E	isomerase		1e-010	7/17	0.028	1.87 ↑	
13E	Elongation factor 2	P29691	2e-009	7/10	0.009	1.74 ↑	Protein biosynthesis
6E	Putative uncharacterized protein	A8WFJ0	5e-009	3/3	0.013	0.60 ↓	////
40E	Vitellogenin-6	P18948	2e-014	19/36	0.026	3.17 ↑	Nutrient reservoir activity
8E	Fructose-1,6-biphosphatase protein 1	Q9N2M2	6e-011	4/7	0.027	4.41 ↑	Energy metabolism
14E	Aconitate hydratase, mitochondrial	P34455	3e-013	6/8	0.039	2.06 ↑	Energy metabolism
38E	Bis (5′-nucleosyl)-tetraphosphatase	Q9U2M7	2e-009	2/2	0.040	1.91 ↑	Apoptosis induction
10E	Heat shock protein 25, isoform a	Q17849	1e-011	4/5	0.049	3.04 ↑	Chaperone
3H	Disorganized muscle protein 1	Q18066	4e-015	16/35	0.035	3.05 ↑	Myofilaments structure
12H	Probable ornithine aminotransferase, mitochondrial	Q18040	2e-015	8/15	0.015	3.09 ↑	Aminoacid biosynthesis
23H	Proteasome subunit beta type-2	P91477	2e-013	5/8	0.017	2.68 ↑	Protein degradation
58H	ATP synthase subunit beta, mitochondrial	P46561	1e-030	31/96	0.033	3.88 ↑	Energy metabolism
61H	Adenylate kinase	Q20140	4e-014	3/4	0.003	72.73 ↑	Energy metabolism
63H	Probable glutaryl-CoA dehydrogenase, mitochondrial	Q20772	8e-007	2/2	0.020	12.24 ↑	Aminoacid metabolism
28H	Fatty acid binding protein 2	Q20224	3e-007	2/10	0.018	35.74 ↑	Fatty acid transport

(*continued*)

Table 1D. Continued

LRRK2 G2019S::Tau vs. *nontransgenic*	*Protein name*	*Swiss prot accession number*	Pb	*Peptides matched/ searched*	P *value*	*Fold increase/ decrease*	*Function*
32H	Guanine nucleotide binding protein beta 2	Q21215	2e-010	8/29	0.036	5.87 ↑	Signaling
34H	ZK829.4 protein	Q23621	2e-006	13/33	0.023	2.60 ↑	Oxidoreductase
40H	Aspartic protease	O76830	2e-009	3/7	0.033	2.56 ↑	Protein degradation

Table 1E

LRRK2 G2019S::Tau vs. *Tau*	*Protein name*	*Swiss prot accession number*	Pb	*Peptides matched/ searched*	P *value*	*Fold increase/ decrease*	*Function*
9E	Fructose-1,6-biphosphatase	Q9N2M2	6e-011	5/7	0.002	2.58↑	Energy metabolism
8E	protein 1		6e-011	4/7	0.030	1.82 ↑	
34E	Triosephosphate isomerase	Q10657	1e-010	7/17	0.017	1.94 ↑	Energy metabolism
28E			7e-011	5/7	0.040	1.83↑	
36E			1e-010	3/4	0.023	7.87 ↑	
27E	GTP-binding nuclear protein	O17915	5e-010	4/9	0.022	0.68 ↓	Nuclear envelope
35E	ran-1		7e-007	2/6	0.048	0.43 ↓	assembly/ cell division
15E	Protein F01G10.1,	O17759	2e-011	11/32	0.024	0.67 ↓	Nematode growth
3E	V-type proton ATPase subunit A	Q9XW92	1e-012	24/45	0.026	2.27 ↑	Lysosome structure, autophagy
7E	60S ribosomal protein L22	P52819	5e-005	2/2	0.027	1.51 ↑	Protein biosynthesis
18E	Arginine kinase F46H5.3	Q10454	1e-010	9/28	0.050	0.63 ↓	Energy metabolism
4H	Heat shock 70 kDa protein F, mitochondrial	P11141	5e-014	7/12	0.029	3.08 ↑	Chaperone
14H	60S Ribosomal protein L6	P47991	2e-009	3/4	0.003	6.56 ↑	Protein biosynthesis
15H	Probable inorganic pyrophosphatase 1	Q18680	6e-013	9/14	0.047	2.49 ↑	Cell growth, development
17H	Vitellogenin-6	P18948	2e-015	19/36	0.005	9.29 ↑	Nutrients reservoir
18H	Actin-1/3	P10983	8e-012	11/21	0.046	9.62 ↑	Cell structure
19H	Enolase	Q27527	6e-016	13/28	0.013	1.73↑	Energy metabolism
20H			7e-016	10/15	0.016	1.88 ↑	
21H	V-type proton ATPase subunit B	Q19626	2e-015	15/31	0.035	3.57 ↑	Lysosome structure, autophagy
22H	Heat shock 70 kDa protein A	P09446	8e-015	14/26	0.049	19.11 ↑	Chaperone
23H	Proteasome subunit beta type-2	P91477	2e-013	5/8	0.025	2.61 ↑	Protein degradation
25H	Eukaryotic translation initiation factor	A8WLV5	9e-011	2/2	0.002	5.85 ↑	Translational process
26H	Methylmalonate-semialdehyde dehydrogenase	P52713	3e-007	2/3	0.046	6.18 ↑	Valine and pyrimidine metabolism
28H	Fatty acid binding protein 2	Q20224	3e-007	2/10	0.047	4.14 ↑	Fatty acid transport
30H	Probable arginine kinase	Q10454	1e-010	9/28	0.038	4.53 ↑	Energy metabolism
32H	Guanine nucleotide binding protein beta 2	Q21215	2e-010	8/29	0.002	6.29 ↑	Signaling
34H	ZK829.4 protein	Q23621	2e-006	13/33	0.011	3.96 ↑	Oxidoreductase
36H	Citrate synthase mitochondrial	P34575	3e-009	10/32	0.027	2.85 ↑	Energy metabolism
37H	Aminopeptidase	Q27245	6e-006	5/13	0.018	16.31 ↑	Protein degradation

Table 1F

LRRK2 R1441C::Tau vs. *non-transgenic*	*Protein name*	*Swiss prot accession number*	Pb	*Peptides matched/ searched*	P *value*	*Fold increase/ decrease*	*Function*
10E	Heat shock protein 25, isoform a	Q17849	1e-011	4/5	0.006	3.52 ↑	Chaperone antioxidant
26E	Triosephosphate isomerase	Q10657	2e-012	9/34	0.008	1.61↑	Energy metabolism
28E			7e-011	5/7	0.028	1.83 ↑	

(*continued*)

TABLE 1F. CONTINUED

LRRK2 R1441C::Tau vs. *non-transgenic*	*Protein name*	*Swiss prot accession number*	Pb	*Peptides matched/ searched*	P *value*	*Fold increase/ decrease*	*Function*
1E	Malate dehydrogenase	Q9UAV5	1e-011	3/5	0.036	3.31↑	Energy metabolism
20E			2e-015	8/31	0.014	1.61↑	
21E			2e-014	4/6	0.031	1.45 ↑	
8E	Fructose-1,6-biphosphatase protein 1	Q9N2M2	6e-011	4/7	0.019	2.42 ↑	Energy metabolism
2E	Histone H4	P62784	3e-006	3/3	0.021	0.62 ↑	Nucleosome structure
41E	Vitellogenin-6	P18948	2e-014	18/36	0.028	2.70 ↑	Nutrient reservoir activity
31E	Fatty-acid and retinol-binding protein 1	P34382	0.0001	2/3	0.028	2.10 ↑	Fatty acid transport
7E	60S ribosomal protein L22	P52819	5e-005	2/2	0.032	3.50 ↑	Protein biosynthesis
32E	Calponin protein 4,	O44727	3e-010	2/3	0.043	1.56 ↑	Muscle structure
22E	Protein F53F1.2,	P91997	3e-013	5/8	0.045	1.63 ↑	Oxidoreductase activity
13E	Elongation factor 2	P29691	2e-009	7/10	0.048	2.15 ↑	Protein biosynthesis
5H	Beta-galactoside-binding lectin	P36573	1e-014	5/13	1.7 E-06	0.03 ↓	Sugar binding
44H	Actin-1/3	P10983	1e-030	20/47	0.020	3.20 ↑	Cell structure
49H	Fructose-bisphosphate aldolase 1	P54216	1e-030	9/19	0.003	9.84 ↑	Energy metabolism
50H			5e-015	6/9			
57H	Tubulin beta-2 chain	P52275	9e-015	19/40	0.005	8.57 ↑	Cell structure
66H	Eukaryotic initiation factor 4A	P27639	3e-015	17/36	0.043	8.62 ↑	Translational process

TABLE 1G

LRRK2 R1441C::Tau vs. *Tau*	*Protein name*	*Swiss prot accession number*	Pb	*Peptides matched/ searched*	P *value*	*Fold increase/ decrease*	*Function*
26E	Triosephosphate isomerase	Q10657	2e-012	9/34	0.003	1.28 ↑	Energy metabolism
3E	V-type proton ATPase catalytic subunit A	Q9XW92	1e-012	24/45	0.007	2.19 ↑	Lysosome structure, autophagy
17E	Fructose-bisphosphate aldolase 1	P54216	5e-014	4/7	0.009	1.69 ↑	Energy metabolism
35E	GTP-binding nuclear protein ran-1	O17915	7e-007	2/6	0.016	1.92 ↑	Nuclear envelope assembly/cell division
2E	Histone H4	P62784	3e-006	3/3	0.022	0.63 ↓	Nucleosome structure
24E	60S ribosomal protein L7	O01802	6e-013	4/7	0.030	1.89 ↑	Protein biosynthesis
30E	Nucleoside diphosphate kinase	Q93576	2e-009	2/4	0.035	0.33 ↓	Synthesis of nucleoside triphosphates
33E	Proteasome subunit alpha type-1	O44156	8e-013	2/2	0.039	1.87 ↑	Protein degradation
31E	Fatty-acid and retinol-binding protein 1	P34382	0.0001	2/3	0.048	1.69 ↑	Fatty acid transport
5E	Myosin regulatory light chain 1	P19625	4e-005	2/3	0.041	1.78 ↑	Muscle structure
1H	60S Ribosomal protein L7	O01802	1e-030	2/4	0.031	12.12 ↑	Protein biosynthesis
14H	60S Ribosomal protein L6	P47991	2e-009	3/4	0.021	15.30 ↑	Protein biosynthesis
17H	Vitellogenin-6	P18948	2e-015	19/36	0.0002	6.04 ↑	Nutrient reservoir
19H	Enolase	Q27527	6e-016	13/28	0.022	2.05 ↑	Energy metabolism
20H			7e-016	10/15	0.041	2.00 ↑	
25H	Eukaryotic translation initiation factor	A8WLV5	9e-011	2/2	0.046	2.37 ↑	Translational process
42H	40S ribosomal protein SA	P46769	6e-014	8/14	0.040	2.62 ↑	Protein biosynthesis
18H	Actin-1/3	P10983	8e-012	11/21	0.004	4.02 ↑	Cell structure
39H	Translationally-controlled tumor protein	Q93573	7e-013	4/15	0.034	30.72 ↑	Microtubule stabilization
40H	Aspartic protease	O76830	2e-009	3/7	0.022	26.12 ↑	Protein degradation

Proteins altered in expression are marked with "E" after the identification number, whereas proteins altered in protein-bound HNE levels are marked with "H" after the identification number. The seven groups of analysis are divided in seven parts of Table 1 marked with alphabetical letters A to G.

†The *p* value listed is the significance of the altered expression or protein-bound HNE levels relative to control samples with $p < 0.05$. *Pb represents the probability of a false identity associated with the identification of each protein using the SEQUEST search algorithm.

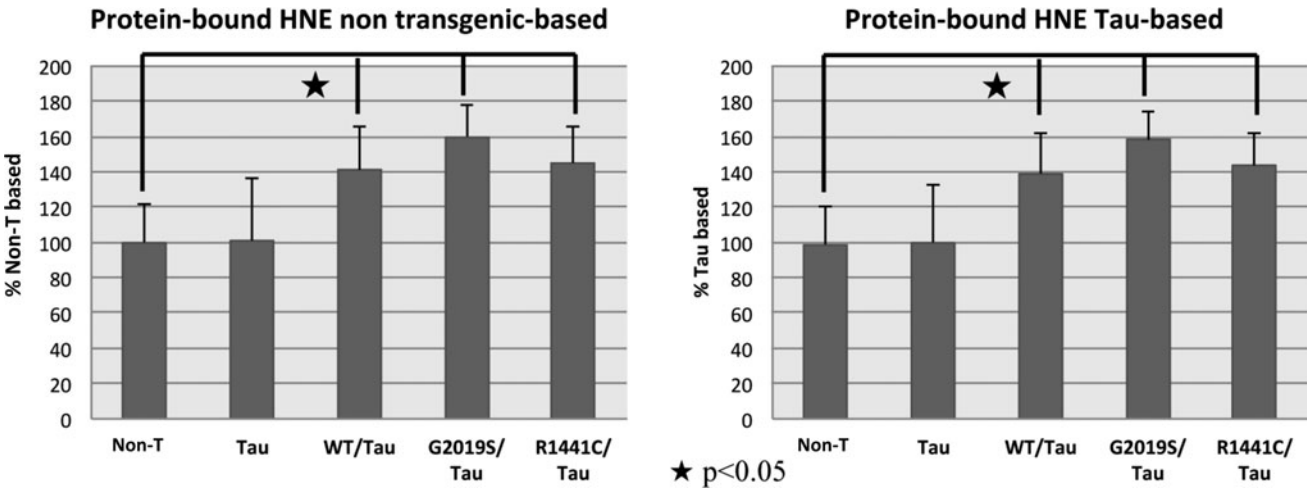

FIG. 4. Bar graph of total protein-bound HNE in *C. elegans* transgenic and nontransgenic strains. Each value was compared before to nontransgenic strain and after to Tau strain, set as 100%. The symbols represent significant differences with p value < 0.05.

LRRK2 R1441C::Tau vs. *Tau*

The proteomics comparison between LRRK2 R1441C::Tau transgenic samples with Tau samples identified increased expression levels of eight proteins (Table 1G; Fig. 4): triosephosphate isomerase (128%), V-type proton ATPase (219%), fructose-bisphosphate aldolase 1 (169%), GTP-binding nuclear protein ran-1 (192), 60S ribosomal protein L7 (189%), proteasome subunit alpha type-1 (187%), fatty-acid and retinol-binding protein 1 (169%), and myosin regulatory light chain 1 (178%); and decreased expression levels of two proteins: histone H4 (63%) and nucleoside diphosphate kinase (33%).

The redox proteomics analysis of protein-bound HNE identified increased levels of nine proteins (Table 1G; Figs. 5 and 6): ribosomal protein L7 (1221%), ribosomal protein L6 (1530%), vitellogenin-6 (604%), enolase (210%, 200%), eukaryotic translation initiation factor (237%), 40S ribosomal protein SA (262%), actin-1/3 (402%), transitionally-controlled tumor protein (307%), and aspartic protease (261%).

Redox proteomics data validation

To verify the proteomics and redox proteomics data, a validation study on expression levels and protein-bound HNE levels of V-type proton ATPase, identified by mass spectrometry analysis in three different groups of analysis, was performed and is shown in Figure 7. V-type proton ATPase was identified with increased expression levels during proteomics analysis in the comparison of LRRK2 G2019S::Tau vs. Tau and LRRK2 R1441C::Tau vs. Tau, and with decreased expression levels in the comparison of LRRK2 WT::Tau vs. Tau. In the redox proteomics analysis, V-type proton ATPase was identified as having increased protein-bound HNE in the comparison of LRRK2 G2019S::Tau vs. Tau. We measured by Western blot the levels of V-type proton ATPase in these

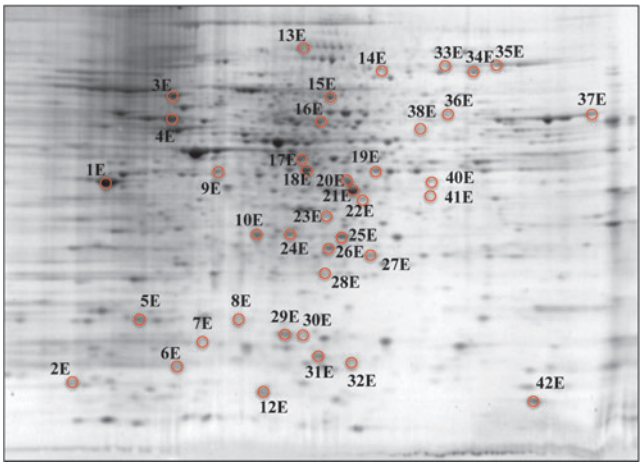

FIG. 5. Representative 2D-gel with all the proteins identified in the expression proteomics study. The proteins are represented with identification numbers followed by the letter "e." Consult Table 1 A–G for results of comparisons among the seven groups. (To see this illustration in color the reader is referred to the web version of this article at www.liebertonline.com/ars).

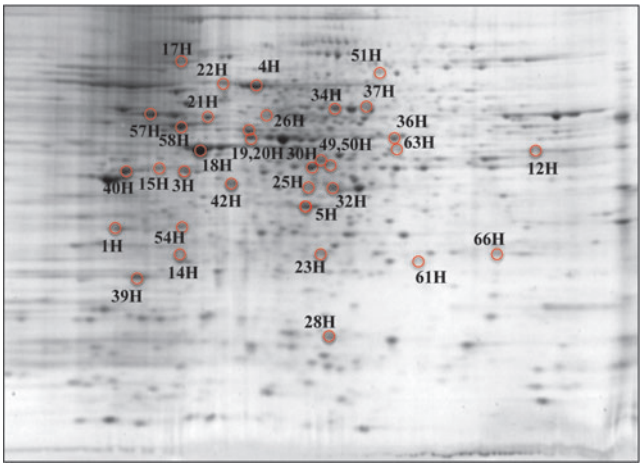

FIG. 6. Representative 2D-gel with all the proteins identified in the redox proteomics study. The proteins are represented with identification numbers followed by the letter "h." Consult Table 1 A–G for results of comparisons among the seven groups. (To see this illustration in color the reader is referred to the web version of this article at www.liebertonline.com/ars).

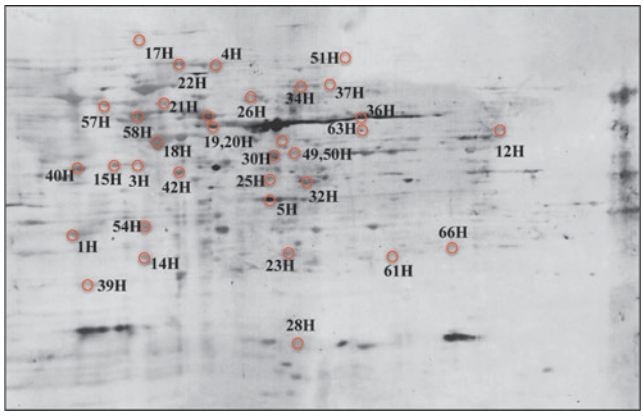

FIG. 7. Representative 2D Western blot with all the proteins identified with altered HNE levels using redox proteomics analysis. (To see this illustration in color the reader is referred to the web version of this article at www.liebertonline.com/ars.)

comparisons and the results are shown in Figure 7. They demonstrate the same trend seen in proteomics analysis for all the comparison groups considered. In detail we show an increase of 183% for LRRK2 G2019S::Tau vs. Tau and of 174% for LRRK2 R1441C::Tau vs. Tau, and an increase of 233% for LRRK2 WT::Tau vs. Tau, confirming the proteomics data.

To validate redox proteomics analysis we immunoprecipitated V-type proton ATPase protein and we performed Western blot analysis probing with anti-HNE antibody to measure specific protein-bound HNE levels. As shown in Figure 7, we found increased protein-bound HNE levels of V-type proton ATPase (310%) in the comparison of LRRK2 G2019S::Tau vs. Tau as we obtained by redox proteomics analysis. The validation studies give confidence in the proteomics identifications presented here.

Increasing autophagic flux reduces deficits in C. elegans *expressing Tau or LRRK2::Tau*

Ridaforolimus is a rapamycin analog able to inhibit mTOR signaling and induce autophagy. To test whether the motor deficits in the *C. elegans* lines were sensitive to the state of autophagy, we examined the effects of ridaforolimus. First, we measured the effect of ridadorolimus on autophagic flux, comparing the results to that observed with rapamycin, a well documented enhancer of autophagic flux. We measured autophagic flux in HEK293 cells expressing mCherry-GFP-LC3 at baseline and in the presence of bafliomycin, a lysosomal inhibitor. In Figures 8A and 8B, we show that ridaforolimus (200 n*M*) increases autophagic flux to the same degree as rapamycin, as evidenced by a loss of GFP-LC3 signal at baseline and recovery of GFP-LC3 signal in the presence of bafliomycin.

In order to test the role of autophagic pathway impairment in our *C. elegans* transgenic models, we administered ridaforolimus to all the strains and measured the thrashes for

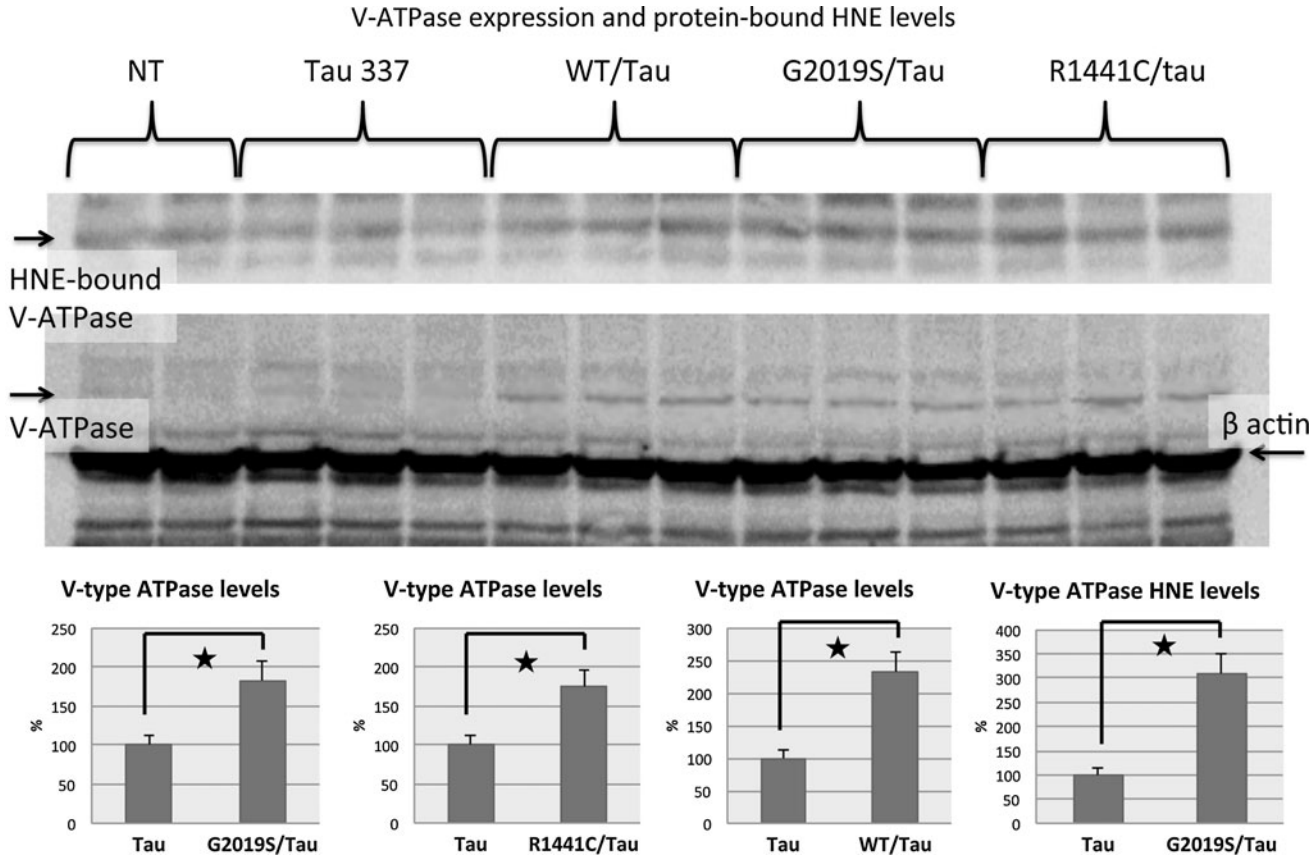

FIG. 8. Proteomics data validation experiments. *Top:* Western blot of expression levels and protein-bound HNE levels of V-type proton ATPase in transgenic and nontransgenic *C. elegans* strains. *Bottom:* Bar graphs of significant differences between the groups analyzed are shown.

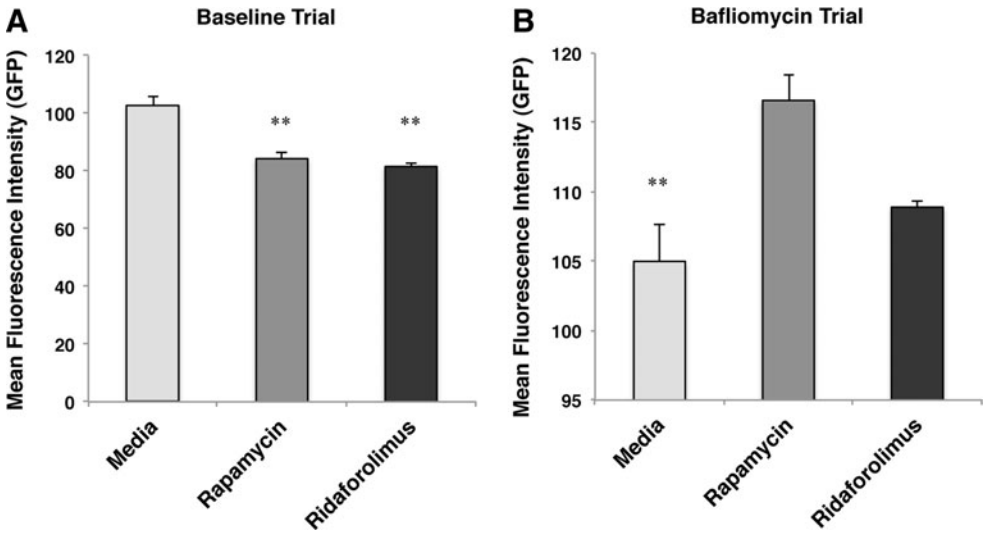

FIG. 9. Comparision of GFP intensity between vehicle, rapamycin (200 n*M*) and ridaforolimus (200 n*M*) without (A) and with (B) bafliomycin; *$p < 0.05$, **$p < 0.01$, ***$p < 0.001$.

30 seconds at day one of adulthood. In Figure 9A we show that ridaforolimus at different concentrations consistently improved thrash number in Tau and LRRK2 R1441C::Tau transgenic strains (as well as in the other transgenic models; data not shown) protecting motor neuron functionality through the restoration of autophagic pathway lost by mutant LRRK2 and tau insertion. In Figure 9B, we show that ridaforolimus maintains its protective activity, at various concentrations, even at 5 days of nematode adulthood, supporting a stable re-establishment of macroautophagy.

Discussion

Increased expression of oxidative markers indexed by increased malondialdehyde-lysine (MDAL) and HNE, increased oxidative damage to selected proteins, with a particular involvement of energy metabolic pathways, have been observed in the cerebral cortex in sporadic PD even at relatively early stages of the disease (9, 10, 12, 21). Past studies, conducted on the involvement of oxidative damage linked to LRRK2 mutations in PD onset and progression, were associated with the G2019S LRRK2 mutation (22). G2019S, and to a lesser degree R1441G, seem crucial for neurite outgrowth, and their expression in primary cortical neurons leads to dramatic reductions in neuritic length and branching of axons and dendrites, loss of dopaminergic neurons, accumulation of abnormal proteins, such as alpha-synuclein and hyper-phosphorylated Tau, together with ubiquitin (17, 43, 48, 61).

A common feature in LRRK2 transgenic models is the presence of Tau alterations that are also present in a subset of LRRK2 patients. An attractive hypothesis is that Tau is one of the downstream targets of LRRK2 kinase activity (31,55). It was proposed that LRRK2 dysfunction impacts on Tau post-translational processing and compartmentalization and thus on its functional roles (14).

In our study we analyzed transgenic *C. elegans* strains expressing human LRRK2 WT, G2019S, and R1441C, and TauV337M genes to study the impact of human WT and mutated LRRK2 together with Tau on protein expression and oxidation. The results of total protein oxidative modifications show a general increase of lipid peroxidation indexed by protein-bound HNE in LRRK2 and TauV337M transgenic (TAU) strains compared to Tau or nontransgenic (Non-T) strains (Fig. 3). These data suggest increased oxidative stress levels involving lipid bilayer components of membranes with the formation of HNE end products that reacts directly with proteins by Michael addition (7). Moreover the presence of WT or mutated LRRK2 with Tau increase the total levels of protein-bound HNE, suggesting a direct or indirect interaction between these proteins as was previously postulated (31, 38, 43, 55).

We also founded a general increase in the levels of protein-bound 3NT (*i.e.*, increased nitration levels) in LRRK2 and Tau strains compared to Non-T, but not to Tau. Protein carbonyls did not show significant differences between LRRK2 and Tau transgenic and nontransgenic strains. Considering the total results on protein oxidation, we chose to focus the redox proteomics analysis on protein-bound HNE in parallel with expression proteomics, mainly because the elevation of this oxidative stress marker was larger than that for 3NT.

Expression and redox proteomics are powerful tools that have been applied to neurodegenerative disorders such as Alzheimer's disease (4, 53) and has been used to identify oxidatively modified proteins in a *C. elegans* model of AD (6). The comparison of the Non-T with Tau strains shows few changes in protein expression, demonstrating slight alteration due to Tau insertion in the genome. The redox proteomics analysis show alteration of proteins mostly involved in energy metabolism or proteolytic pathways, but the undefined trend of oxidation towards one or the other group and the relative small number of proteins identified establish again a minor impact of the presence of Tau on cell redox status as seen alone for total oxidation levels. Accounting for these results, we propose that the overexpression of Tau by itself does not determine significant alterations on *C. elegans* protein expression and oxidation levels; however, this condition might change in the presence of others factors that could interact with Tau.

To test the hypothesis of association between WT and mutated LRRK2 and Tau in PD onset and development, we analyzed by proteomics and redox proteomics transgenic *C. elegans* strains containing human LRRK2 (WT, G2019S, and R1441C) and Tau genes compared to either Tau or Non-T.

The LRRK2 WT::Tau strain demonstrated changes in the expressions levels of 11 and 12 proteins in the comparison with Non-T and Tau strains, respectively. Indeed, both the comparison groups displayed alterations of similar molecular pathways. Interestingly, many of the altered proteins, such as glyceraldehyde-3-phosphate dehydrogenase, are involved in the glucose metabolism pathway, suggesting glycolysis as a consistent target of LRRK2::Tau interaction in the *C. elegans* model. However, proteomics data show also the common alteration of proteins involved in apoptotic processes as well as nucleosome and ribosome structure, suggesting these specific pathways are also involved in the alterations. The altered protein-bound HNE levels were identified in, among the other proteins, ribosomal protein L7 and heat shock 70 kDa protein in the comparison of WT::TAU with TAU and in proteasome subunit alpha type-5 and 40S ribosomal protein SA in the comparison with Non-T. Some of the oxidized proteins identified by redox proteomics belong to molecular pathways also altered in the expression proteomics analysis. However, in both the groups of matching there is no clear trend of oxidation.

The overall proteomics and redox proteomics data suggest that the expression of LRRK2 WT with Tau does not have a strong impact on expression levels and protein oxidation in *C. elegans*. LRRK2 WT by itself, and in correlation with Tau is not able to cause large changes in the proteome, and the supposed downstream control that LRRK2 has on Tau PTM seems not to be altered when LRRK2 is not mutated. However, alteration of proteins involved in protein folding, biosynthesis, and degradation might depend by LRRK2 expression only and correlates with previous studies. A number of reports suggest a role for LRRK2 in regulating neuronal responses to stress, and in *C. elegans* it was reported that WT LRRK2 protects against mitochondrial dysfunction, but disease-related mutants of LRRK2 appear to produce responses that range from less protection to overt enhancement of toxicity (47). The co-expression of mutated LRRK2 (G2019S or R1441C) with Tau showed a higher effect on protein expression alterations and protein oxidation than WT::Tau co-expression for the number of proteins and molecular pathways involved and mainly for the trend of oxidatively modified proteins that clearly shifted towards the mutated forms. The expression profile of the *C. elegans* strain expressing LRRK2 G2019S::Tau compared both to Tau and Non-T strains demonstrate the alteration of 8 and 11 proteins, respectively, with several common identifications. In fact, changes in expression of proteins involved with energy metabolism are highly shared in both matching groups. This result was obtained also in the comparison with WT::Tau, confirming once again that LRRK2::Tau interaction consistently affects glucose metabolic pathways. Indeed, other proteins in the comparison of mutated LRRK2::Tau with Tau or Non-T display expression levels alterations such as ribosomal proteins, and interestingly cell structure proteins. These two groups of proteins are both shared between the two mutations considered and in common with the previous comparison group. The expression proteomics results show that the alterations in expression are mainly induced by the co-expression of LRRK2 (mutated or WT) with Tau that largely affect similar molecular pathways such as metabolic pathways, cell structure, or protein biosynthesis and degradation. However, a substantial difference between the co-expression of WT::Tau and mutated::Tau compared to control groups is that the expression levels mostly shift towards protein overexpression in presence of the mutations.

The redox proteomics results regarding protein-bound HNE show increased protein oxidative modification in strains with co-expression of mutated/tau compared to Tau, or Non-T. For G2019S::Tau we found increased HNE levels in 17 proteins compared to Tau, and 10 proteins in the comparison with Non-T. The number of proteins oxidatively modified identified by redox proteomics is consistent with the results of the total HNE levels, demonstrating increased lipid peroxidation in the presence of G2019S::Tau. In DA neurons, it was reported that the LRRK2 G2019S dominant mutant causes several dendritic defects, including Tau mislocalization, Tau hyperphosphorylation, and dendrite degeneration with the same behavior of Tau overexpression in DA neurons. Moreover, the co-expression of G2019S and Tau leads to neuronal loss and lack of microtubules in dendrites more intensely than either one alone (31). Hence, as Lin *et al*. suggested previously (31), our data support the notion that the interaction of mutated LRRK2 with Tau induces and enhances the detrimental activities of Tau in neurodegeneration.

Based on the identified proteins in expression proteomics analysis, one of the main pathways affected by G2019S::Tau expression is energy metabolism. These data correlate with previous studies on PD models about the oxidation of energy metabolism enzymes such as enolase (21), strengthening our *C. elegans* model as an appropriate PD model.

The R1441C/TAU co-expression present similar results to those to G2019S::Tau co-expression, suggesting common mechanisms that lead to increased oxidative stress.

The R1441C::Tau co-expression identified HNE modification of 4 and 9 proteins in the comparison with Tau and Non-T strains, respectively. The oxidative modifications affect metabolic proteins, but also like other LRRK2 transgenic strains, structural proteins and protein involved in protein biosynthesis and degradation are affected.

The redox proteomics data are consistent with the notion that the trend of oxidation is a result of the interaction of mutated LRRK2 and Tau. Mutated LRRK2 might increase its activity in a mechanism of gain of function (58), triggering the activation of several downstream signals that lead to Tau hyperphosphorylation and increased oxidative stress.

Analyzing specific protein alterations, this study reveals the different expression and the increased protein-bound HNE levels of several proteins involved in the autophagy process during the co-expression of LRRK2 WT or mutated and Tau. Recently, autophagy is gaining attention for its potential contribution to the pathogenesis of several neurodegenerative diseases (36, 41, 46). The increase in autophagic vacuoles in the substantia nigra of PD brains (5) supports the idea that autophagy is involved in PD. Several factors are implicated in autophagy alterations in PD, and recently Plowey *et al.* (42) suggested a strong link between LRRK2 and autophagy, consistent with an active role for autophagy induced by the LRRK2 pathological mutant. Expression of LRRK2 G2019S or R1441C leaded to the accumulation of increased autophagic vacuoles (2, 42). Here we found alteration of V-type proton ATPase, a vacuolar proton pump involved in lysosomal autophagy, in the presence of LRRK2::Tau co-expression. Supporting our results, it was previously reported that increased oxidative stress could affect the permeability of the lysosomal membrane

or damage the lysosomal membrane by oxidizing proteins (60). Moreover, the findings that lysosomal malfunction (39) and mutations in ATP13A2, a lysosomal ATPase, led to a failure of autophagy execution in PD (15, 44) strengthen the correlation between LRRK2, autophagy and PD.

The further use of ridaforolimus supported our proteomics and redox proteomics results and is consistent with the notion of autophagic impairment in LRRK2/Tau transgenic strains. Ridaforolimus is a rapamycin analog and a macroautophagy activator through its inhibition of mTOR signaling (45, 52). We report in the present study a restoration of motor neuron functionality in the presence of ridaforolimus, through improved autophagy, in young and aged strains. Thus, by testing ridaforolimus in our nematode transgenic models, we confirmed both the involvement of autophagy impairment in mutated LRRK2 and Tau-modulated neurodegeneration and the potent protective effect of ridaforolimus against disease-associated mutant protein toxicity.

We also found in our study the altered expression and oxidative modification of several proteasome subunits during co-expression of LRRK2 WT or mutated and Tau. This result suggests that not only the autophagic way of protein degradation might be impaired by LRRK2 expression, but also the ubiquitin/proteasome system leading to the formation of protein aggregates as seen for the mutations of parkin (18) and UCH- L1 (35) components of the system. Increased oxidative stress, associated with depletion of ATP, is thought to contribute to the reduction of proteasome activity and aggregation of abnormal proteins (1, 32). The energy-related proteins identified in this study are consistent with this notion. It is generally believed that autophagy and the ubiquitin/proteasome system operate in concert playing a vital role in homeostasis and the cellular responses to stresses, such as endoplasmic reticulum stress, and mitochondrial damage.

Further, we identified various mitochondrial proteins, some energy-related and some not, such as NADH ubiquinone oxidoreductase protein 2 (LRRK2 specific) or mitochondrial HSP 70, that might suggest alterations and injury of the mitochondria. Dysfunction of mitochondria is implicated in the pathophysiology of PD (49, 56), and recent studies raised the possibility that LRRK2 modulates mitochondrial function and impairment (47). The increased expression of NADH ubiquinone oxidoreductase protein 2 is particularly interesting because it provides a mechanism through which LRRK2 might protect against rotenone, which we demonstrated previously (47). Upregulation of NADH ubiquinone oxidoreductase protein 2 would increase activity of complex I of the electron transport chain, which could protect against the deleterious effects of rotenone. Damaged mitochondria are a well-known source of pro-oxidant species, and mitophagy is thought to be a crucial process to protect cells from mitochondrial leakage of ROS/RNS. We suppose that the alterations of mitochondrial proteins could probably be related to changes in mitochondrial turnover (mitophagy) that are implicated for parkin and PINK1, and might be relevant to LRRK2.

We also reported cell structure impairment linked to LRRK2 expression for the alterations on actin depolymerizing factor 2 in LRRK2 WT::Tau, actin 1/3 and tubulin beta-2 chain in LRRK2 G2019S:: or R1441C::Tau. These findings nicely correlate with a recent study by Chen *et al.* showing regulation of LRRK2 by rac1 and linkage to actin remodeling (8). Moreover, three members of the ezrin/radixin/moesin (ERM) family, which regulate actin cytoskeleton reorganization and membrane curvature dynamics, are among the few recognized substrates of LRRK2 (3).

Another very interesting result concerns the involvement of protein biosynthetic machinery in the detrimental influence of LRRK2 and Tau co-expression in *C. elegans* transgenic strains. We identified here alterations of the eukaryotic translation initiation factor LRRK2 G2019S:: and R1441C::Tau and of eukaryotic initiation factor 4A LRRK2 R1441C::Tau that are part of the translational machinery. Moreover, we show altered expression and increased oxidation of several ribosomal subunits in most of the transgenic strains analyzed. A previous study by Imai *et al*. (25) reported 4E-BP, an interactor of the eukaryotic protein translation initiation factor eIF4E that in turn binds to capped mRNA species promoting their translation, as a potential substrate of LRRK2. LRRK2 phosphorylation of 4E-BP modulates the binding to eIF4E, controlling the repression of translation.

In conclusion, the co-expression of human WT LRRK2 and Tau lead to protein expression changes without altering the redox status, while mutated LRRK2 leads to increased protein oxidation. This result suggests that LRRK2 might interact with Tau through the activation of several downstream signals and the mutation could enhance LRRK2 effects on tau PTM and compartmentalization. Interestingly, we show that LRRK2 expression affects protein biosynthesis and degradation, and the mutations appear to enhance this unfavorable outcome. Involvement of protein degradation pathways, with a special attention on autophagy, in LRRK2 mediated degenerative process is gaining wide interest as a PD causative agent and represents a fascinating result of our study.

Materials and Methods

Chemicals

Ridaforolimus was supplied by ARIAD Pharmaceuticals (Cambridge, MA). All other chemicals were purchased from Sigma (Sigma, St Louis, MO), unless otherwise indicated.

Nematode culture and transgenic crossing

All LRRK2 lines were generated in the Wolozin Laboratory as previously described (47). The Tau V337M strain was generated and generously shared by Dr. Brian Kraemer of the University of Washington. The Bristol strain N2 was the nontransgenic line. Nematodes strains were grown at 20°C on standard NGM plates coated with a thin layer of OP50 bacteria. Crosses were produced by mating male LRRK2 lines with hermaphrodites from the Tau V337M lines. Progeny were examined by PCR for the presence of LRRK2 and propagated until homozygotes could be identified (Fig. 10). Liquid thrashing assays were performed in 20 (l of water on the lid of a plastic Petri dish. Age-synchronized worms were allowed to settle, and thrashes were counted for three 30 second intervals ($n = 10$ per group).

Primer sets

LRRK2 - forward - 5′-ATG GCT AGT GGC AGC TGT CAG-3′
LRRK2 - reverse - 5′-GAG TCC AAG ACG ATC AAC AGA-3′
Tau - forward - 5′-CAA GCT CGC ATG GTC AGT AA-3′
Tau - reverse - 5′-TTC TCA GTG GAG CCG ATC TT-3′

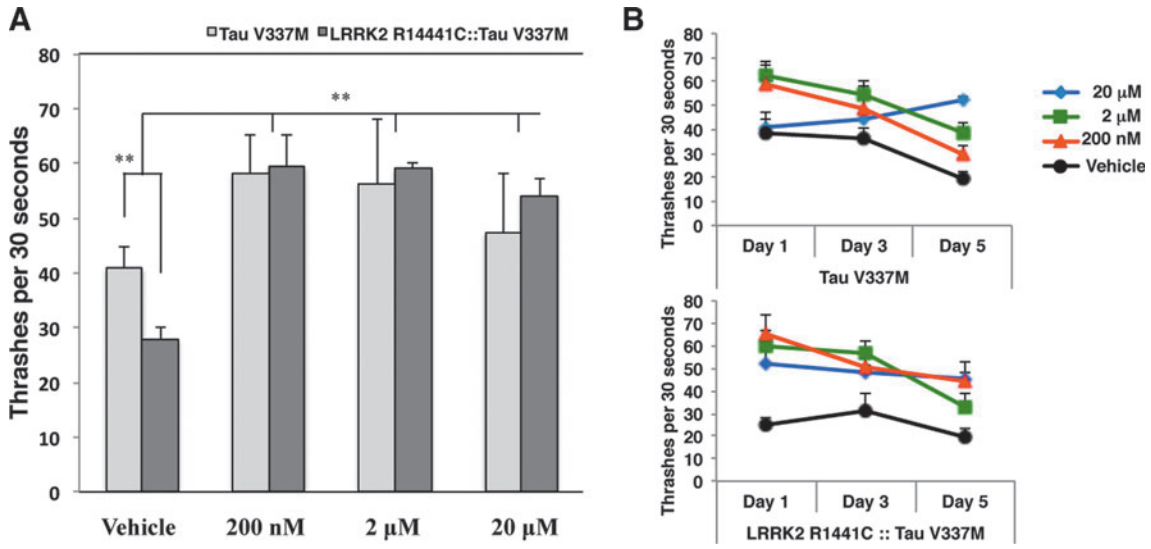

FIG. 10. Age synchronized nematodes cultured with varied doses of ridaforolimus. (A) Movement (thrashing) assessed on day 1 of adulthood. $^{**}p < 0.01$; **(B)** movement (thrashing) assessed on day 1, 3, and 5 of adulthood. (To see this illustration in color the reader is referred to the web version of this article at www.liebertonline.com/ars).

Sample preparation

The lyophilized samples were manually homogenized in ice-cold buffer (10 m*M* Tris pH 8, 0.32 *M* Sucrose, 0.1 m*M* MgCl2, 0.1 m*M* ethylenediaminetetraacetic acid, 10 μg/ml leupeptin, 10 μg/ml pepstatin, 10 μg/ml aprotinin) and sonicated for 10 sec on ice. Protein concentration was determined by the BCA method (Pierce, Rockford, IL). Proteins (150 (g) were precipitated in 15% final concentration of trichloroacetic acid for 10 min in ice. Samples were then spun down at 14000 rpm for 5 min, and precipitates were washed in ice-cold ethanol-ethyl acetate 1:1 solution four times.

The final pellets were dissolved in 200 μl of 8 *M* urea, 2% CHAPS, 2 *M* thiourea, 20 m*M* dithiothreitol, 0.2% of amopholytes (Bio-Rad, Hercules, CA) and bromophenol blue, incubated at room temperature for 90 min and sonicated for 5 sec.

Protein oxidation analysis

Total protein carbonyls, protein-bound HNE, and protein-bound 3NT levels were analyzed by slot blot method. Briefly, for protein carbonyls, the samples (5 (g of protein) were derivatized with 10 m*M* 2,4-dinitrophenylhydrazine in the presence of 5 (l of 12% SDS for 20 min at room temperature. The samples were neutralized with 7.5 (l of the neutralization solution (2 *M* Tris in 30% glycerol). The resulting solution was loaded into each well on nitrocellulose membrane under vacuum using a slot-blot apparatus (250 ng/lane). The membrane then was washed with wash buffer [10 m*M* Tris–HCl (pH 7.5), 150 m*M* NaCl, 0.05% Tween 20], blocked by incubation in the presence of 3% BSA, followed by incubation with rabbit polyclonal anti-DNPH antibody as primary antibody for 1 h. The membrane was washed with wash buffer and further incubated with alkaline phosphatase (ALP)-conjugated goat anti-rabbit antibody as secondary antibody for 1 h. The blot was developed using 5-bromo-4-chloro-3-indolyl-phosphate/nitroblue tetrazolium (BCIP/NBT) color developing reagent, scanned in TIF format using Adobe Photoshop on a Canoscan 8800F (Canon, USA) and quantified with ImageQuant TL 1D version 7.0 software (GE Healthcare, USA).

2D electrophoresis and blotting

Samples (200 μl, 200 μg) were loaded on 110-mm pH 3–10 immobilized pH gradients (IPG) strips in a Bio-Rad IEF Cell system (Bio-Rad). Following 18 h of active rehydration (50 V) isoelectric focusing was performed. For the second dimension, thawed strips were sequentially equilibrated for 15 min in the dark in 375 m*M* Tris pH 8.8, 6 *M* urea, 2% sodium dodecyl sulfate (SDS), 20% glycerol containing first 2% dithiothreitol and then 2.5% of iodoacetamide. SDS PAGE was performed in Criterion Tris-HCl Gels 8-16% (Bio-Rad) at 200 V for 1 h. Gels were fixed for 45 min in 10% methanol, 7% acetic acid, and stained overnight on the rocker with SYPRO Ruby gel stain (Bio-Rad). After destaining in deionized water, gels were scanned with a STORM UV transilluminator (λex = 470 nm, λem = 618 nm, Molecular Dynamics, Sunnyvale, CA).

The same amount of protein sample (200 μg) was used for 2D- immunoblotting analysis, and the electrophoresis was carried out as described above. The proteins from the 2D-electrophoresis gels were transferred to nitrocellulose membranes (Bio-Rad) using a Transblot-Blot SD Semi-Dry Transfer Cell (Bio-Rad) at 15 V for 2 h. HNE-protein adducts were detected on the nitrocellulose paper using a primary anti-HNE rabbit antibody (Chemicon, Temecula, CA) specific for HNE-bound protein (1:100) for 2 h at room temperature while rocking, followed by a secondary goat anti-rabbit IgG (Sigma) antibody (1:1300) diluted in wash blot buffer for 2 h RT. The resultant membrane was developed as previously described.

PD-Quest analysis

Gel imaging was software-aided using PD-Quest (Bio-Rad) imaging software. Briefly, a master gel was selected followed by normalization of all gels (nontransgenic and transgenic

strain samples), according to the total spot density. Gel-to-gel analysis was then initiated in two parts: manual matching and automated matching. This process generates a large pool of data, approximately 350 spots. Only proteins showing computer-determined significant differential levels between the two groups being analyzed were considered for identification. A quantitative analysis set was created that recognized matched spots with differences in the number of pixels that occur in each spot and a statistical analysis set was created that used a Student's *t*-test at 95% confidence to identify spots with p values of <0.05. Spots with $p<0.05$ were considered significant. A Boolean analysis set was created that identified overlapping spots from the aforementioned quantitative and statistical sets. These spots were selected for subsequent mass spectrometric analysis.

Gel cutting and in-gel trypsin digestion

Protein spots statistically different than controls were digested in-gel by trypsin. Briefly, spots of interest were excised and then washed with 0.1 *M* ammonium bicarbonate (NH_4HCO_3) at room temperature for 15 min. Acetonitrile was added and incubated at room temperature for 15 min. This solvent mixture was then removed and gel pieces dried. The protein spots were then incubated with 20 μl of 20 m*M* DTT in 0.1 *M* NH_4HCO_3 at 56°C for 45 min. The DTT solution was removed and replaced with 20 μl of 55 m*M* iodoacetamide in 0.1 *M* NH_4HCO_3. The solution was then incubated at room temperature for 30 min. The iodoacetamide was removed and replaced with 0.2 ml of 50 m*M* NH_4HCO_3 at room temperature for 15 min. Acetonitrile (200 μl) was added. After 15 min incubation, the solvent was removed, and the gel spots were dried for 30 min. The gel pieces were rehydrated with 20 ng/μl-modified trypsin (Promega, Madison, WI) in 50 m*M* NH_4HCO_3 with the minimal volume enough to cover the gel pieces. The gel pieces were incubated overnight at 37°C in a shaking incubator.

Mass spectrometry

Protein spots of interest were excised, subjected to in-gel trypsin digestion, and resulting tryptic peptides were analyzed with an automated nanospray Nanomate Orbitrap XL MS/MS platform (6). The Orbitrap MS was operated in a data-dependent mode whereby the 8 most intense parent ions measured in the FT at 60,000 resolution were selected for ion trap fragmentation with the following conditions: injection time 50 ms, 35% collision energy. MS/MS spectra were measured in the FT at 7500 resolutions, and dynamic exclusion was set for 120 seconds. Each sample was acquired for a total of $\sim$2.5 min. MS/MS spectra were searched against the ipi Worms Database using SEQUEST with the following criteria: Xcorr > 1.5, 2.0, 2.5, 3.0 for +1, +2, +3, and +4 charge states, respectively, and P-value (protein and peptide) < 0.01. IPI accession numbers were cross-correlated with SwissProt accession numbers for final protein identification.

Western blot analysis

Proteins (50 μg) were added to sample buffer, denaturated for 5 min at 100°C, loaded on 8%–16 % precast Criterion gels (Bio-Rad) and separated by electrophoresis at 100 mA for 2 h. The gels were then transferred to nitrocellulose paper using the Transblot-BlotSD Semi-DryTransfer Cell at 20 mA for 2 h. The membranes were incubated with V-type proton ATPase mouse monoclonal primary antibody (AbCam) for expression analysis in PBST for 2 h at room temperature. The membranes were then washed three times for 5 min with PBST, followed by incubation with anti-mouse alkaline phosphatase secondary antibody (Sigma) in PBST for 2 h at room temperature. Membranes were then washed, developed, and scanned as previously described.

Immunoprecipitation

For the immunoprecipitation procedure, 150 μg of protein extracts were dissolved in 500 μl of RIPA buffer (10 m*M* Tris, pH 7.6; 140 m*M* NaCl; 0.5% NP40 including protease inhibitors) and then incubated with 1 μg of V-type proton ATPase antibody at 4°C overnight. Immunocomplexes were collected by using protein A/G suspension for 2 h at 4°C and washed five times with immunoprecipitation buffer. Immunoprecipitated V-type proton ATPase was recovered by resuspending the pellets in reducing SDS buffers and subjected to electrophoresis on 12% gels, followed by Western blot analysis.

Statistical analysis

Statistical analysis of protein levels matched with spots on 2D-gels from mutated LRRK2::Tau transgenic strains compared Non-T and Tau transgenic strains were carried out using Student's *t*-tests. A value of $p<0.05$ was considered statistically significant. Only proteins that were considered significantly different by Student's *t*-test were subjected to in-gel trypsin digestion and subsequent proteomic analysis.

Acknowledgments

This work was supported in part by grants to DAB (NIH AG-05119) and to BW (Alzheimer Association, NIEHS ES15567, NINDS NS060872). FDD was supported by a Fellowship from Istituto Pasteur–Fondazione Cenci Bolognetti.

Author Disclosure Statement

The authors state no financial conflict of interests in this study.

References

1. Abou-Sleiman PM, Muqit MM, and Wood NW. Expanding insights of mitochondrial dysfunction in Parkinson's disease. *Nat Rev Neurosci* 7: 207–219, 2006.
2. Alegre-Abarrategui J, Christian H, Lufino MM, Mutihac R, Venda LL, Ansorge O, and Wade-Martins R. LRRK2 regulates autophagic activity and localizes to specific membrane microdomains in a novel human genomic reporter cellular model. *Hum Mol Genet* 18: 4022–4034, 2009.
3. Alegre-Abarrategui J and Wade-Martins R. Parkinson disease, LRRK2 and the endocytic-autophagic pathway. *Autophagy* 5: 1208–1210, 2009.
4. Aluise CD, Robinson RA, Cai J, Pierce WM, Markesbery WR, and Butterfield DA. Redox proteomics analysis of brains from subjects with amnestic mild cognitive impairment compared to brains from subjects with preclinical Alzheimer's disease: Insights into memory loss in MCI. *J Alzheimers Dis* 23: 257–269, 2011.
5. Anglade P, Vyas S, Javoy-Agid F, Herrero MT, Michel PP, Marquez J, Mouatt-Prigent A, Ruberg M, Hirsch EC, and Agid Y. Apoptosis and autophagy in nigral neurons of patients with Parkinson's disease. *Histol Histopathol* 12: 25–31, 1997.

6. Boyd-Kimball D, Poon HF, Lynn BC, Cai J, Pierce WM, Jr., Klein JB, Ferguson J, Link CD, and Butterfield DA. Proteomic identification of proteins specifically oxidized in *Caenorhabditis elegans* expressing human Abeta(1-42): Implications for Alzheimer's disease. *Neurobiol Aging* 27: 1239–1249, 2006.
7. Butterfield DA, Bader Lange ML, and Sultana R. Involvements of the lipid peroxidation product, HNE, in the pathogenesis and progression of Alzheimer's disease. *Biochim Biophys Acta* 1801: 924–929, 2010.
8. Chan D, Citro A, Cordy JM, Shen GC, and Wolozin B. Rac1 Protein rescues neurite retraction caused by G2019S leucine-rich repeat kinase 2 (LRRK2). *J Biol Chem* 286: 16140–16149, 2011.
9. Choi J, Levey AI, Weintraub ST, Rees HD, Gearing M, Chin LS, and Li L. Oxidative modifications and down-regulation of ubiquitin carboxyl-terminal hydrolase L1 associated with idiopathic Parkinson's and Alzheimer's diseases. *J Biol Chem* 279: 13256–13264, 2004.
10. Choi J, Rees HD, Weintraub ST, Levey AI, Chin LS, and Li L. Oxidative modifications and aggregation of Cu,Zn-superoxide dismutase associated with Alzheimer and Parkinson diseases. *J Biol Chem* 280: 11648–11655, 2005.
11. Dachsel JC and Farrer MJ. LRRK2 and Parkinson disease. *Arch Neurol* 67: 542–547, 2010.
12. Dalfo E, Portero-Otin M, Ayala V, Martinez A, Pamplona R, and Ferrer I. Evidence of oxidative stress in the neocortex in incidental Lewy body disease. *J Neuropathol Exp Neurol* 64: 816–830, 2005.
13. Dalle-Donne I, Scaloni A, and Butterfield DA. *Redox Proteomics: From Protein Modifications to Cellular Dysfunction and Diseases* New York: John Wiley and Sons; 2006.
14. Devine MJ and Lewis PA. Emerging pathways in genetic Parkinson's disease: Tangles, Lewy bodies and LRRK2. *FEBS J* 275: 5748–5757, 2008.
15. Di Fonzo A, Chien HF, Socal M, Giraudo S, Tassorelli C, Iliceto G, Fabbrini G, Marconi R, Fincati E, Abbruzzese G, Marini P, Squitieri F, Horstink MW, Montagna P, Libera AD, Stocchi F, Goldwurm S, Ferreira JJ, Meco G, Martignoni E, Lopiano L, Jardim LB, Oostra BA, Barbosa ER, Italian Parkinson Genetics N, and Bonifati V. ATP13A2 missense mutations in juvenile parkinsonism and young onset Parkinson disease. *Neurology* 68: 1557–1562, 2007.
16. Farrer MJ. Genetics of Parkinson disease: Paradigm shifts and future prospects. *Nat Rev Genet* 7: 306–318, 2006.
17. Forno LS. Neuropathology of Parkinson's disease. *J Neuropathol Exp Neurol* 55: 259–272, 1996.
18. Foroud T, Uniacke SK, Liu L, Pankratz N, Rudolph A, Halter C, Shults C, Marder K, Conneally PM, Nichols WC, and Parkinson Study G. Heterozygosity for a mutation in the parkin gene leads to later onset Parkinson disease. *Neurology* 60: 796–801, 2003.
19. Galpern WR and Lang AE. Interface between tauopathies and synucleinopathies: A tale of two proteins. *Ann Neurol* 59: 449–458, 2006.
20. Gloeckner CJ, Schumacher A, Boldt K, and Ueffing M. The Parkinson disease-associated protein kinase LRRK2 exhibits MAPKKK activity and phosphorylates MKK3/6 and MKK4/7, *in vitro. J Neurochem* 109: 959–968, 2009.
21. Gomez A and Ferrer I. Increased oxidation of certain glycolysis and energy metabolism enzymes in the frontal cortex in Lewy body diseases. *J Neurosci Res* 87: 1002–1013, 2009.
22. Gomez A and Ferrer I. Involvement of the cerebral cortex in Parkinson disease linked with G2019S LRRK2 mutation without cognitive impairment. *Acta Neuropathol* 120: 155–167, 2010.
23. Guthrie CR, Schellenberg GD, and Kraemer BC. SUT-2 potentiates tau-induced neurotoxicity in *Caenorhabditis elegans*. *Hum Mol Genet* 18: 1825–1838, 2009.
24. Hatano T, Kubo S, Imai S, Maeda M, Ishikawa K, Mizuno Y, and Hattori N. Leucine-rich repeat kinase 2 associates with lipid rafts. *Hum Mol Genet* 16: 678–690, 2007.
25. Imai Y, Gehrke S, Wang HQ, Takahashi R, Hasegawa K, Oota E, and Lu B. Phosphorylation of 4E-BP by LRRK2 affects the maintenance of dopaminergic neurons in *Drosophila*. *EMBO J* 27: 2432–2443, 2008.
26. Kraemer BC, Burgess JK, Chen JH, Thomas JH, and Schellenberg GD. Molecular pathways that influence human tau-induced pathology in Caenorhabditis elegans. *Hum Mol Genet* 15: 1483–1496, 2006.
27. Kraemer BC, Zhang B, Leverenz JB, Thomas JH, Trojanowski JQ, and Schellenberg GD. Neurodegeneration and defective neurotransmission in a *Caenorhabditis elegans* model of tauopathy. *Proc Natl Acad Sci USA* 100: 9980–9985, 2003.
28. Lewis PA, Greggio E, Beilina A, Jain S, Baker A, and Cookson MR. The R1441C mutation of LRRK2 disrupts GTP hydrolysis. *Biochem Biophys Res Commun* 357: 668–671, 2007.
29. Li X, Tan YC, Poulose S, Olanow CW, Huang XY, and Yue Z. Leucine-rich repeat kinase 2 (LRRK2)/PARK8 possesses GTPase activity that is altered in familial Parkinson's disease R1441C/G mutants. *J Neurochem* 103: 238–247, 2007.
30. Li Y, Dunn L, Greggio E, Krumm B, Jackson GS, Cookson MR, Lewis PA, and Deng J. The R1441C mutation alters the folding properties of the ROC domain of LRRK2. *Biochim Biophys Acta* 1792: 1194–1197, 2009.
31. Lin CH, Tsai PI, Wu RM, and Chien CT. LRRK2 G2019S mutation induces dendrite degeneration through mislocalization and phosphorylation of tau by recruiting autoactivated GSK3ss. *J Neurosci* 30: 13138–13149, 2010.
32. Lin MT and Beal MF. Mitochondrial dysfunction and oxidative stress in neurodegenerative diseases. *Nature* 443: 787–795, 2006.
33. Ludolph AC, Kassubek J, Landwehrmeyer BG, Mandelkow E, Mandelkow EM, Burn DJ, Caparros-Lefebvre D, Frey KA, de Yebenes JG, Gasser T, Heutink P, Hoglinger G, Jamrozik Z, Jellinger KA, Kazantsev A, Kretzschmar H, Lang AE, Litvan I, Lucas JJ, McGeer PL, Melquist S, Oertel W, Otto M, Paviour D, Reum T, Saint-Raymond A, Steele JC, Tolnay M, Tumani H, van Swieten JC, Vanier MT, Vonsattel JP, Wagner S, and Wszolek ZK, Reisensburg Working Group for Tauopathies With P. Tauopathies with parkinsonism: Clinical spectrum, neuropathologic basis, biological markers, and treatment options. *Eur J Neurol* 16: 297–309, 2009.
34. MacLeod D, Dowman J, Hammond R, Leete T, Inoue K, and Abeliovich A. The familial Parkinsonism gene LRRK2 regulates neurite process morphology. *Neuron* 52: 587–593, 2006.
35. Maraganore DM, Lesnick TG, Elbaz A, Chartier-Harlin MC, Gasser T, Kruger R, Hattori N, Mellick GD, Quattrone A, Satoh J, Toda T, Wang J, Ioannidis JP, de Andrade M, and Rocca WA, Consortium UGG. UCHL1 is a Parkinson's disease susceptibility gene. *Ann Neurol* 55: 512–521, 2004.
36. Martinez-Vicente M and Cuervo AM. Autophagy and neurodegeneration: When the cleaning crew goes on strike. *Lancet Neurol* 6: 352–361, 2007.
37. Mata IF, Wedemeyer WJ, Farrer MJ, Taylor JP, and Gallo KA. LRRK2 in Parkinson's disease: Protein domains and functional insights. *Trends Neurosci* 29: 286–293, 2006.
38. Melrose HL, Dachsel JC, Behrouz B, Lincoln SJ, Yue M, Hinkle KM, Kent CB, Korvatska E, Taylor JP, Witten L,

Liang YQ, Beevers JE, Boules M, Dugger BN, Serna VA, Gaukhman A, Yu X, Castanedes-Casey M, Braithwaite AT, Ogholikhan S, Yu N, Bass D, Tyndall G, Schellenberg GD, Dickson DW, Janus C, and Farrer MJ. Impaired dopaminergic neurotransmission and microtubule-associated protein tau alterations in human LRRK2 transgenic mice. *Neurobiol Dis* 40: 503–517, 2010.
39. Meredith GE, Totterdell S, Petroske E, Santa Cruz K, Callison RC, Jr., and Lau YS. Lysosomal malfunction accompanies alpha-synuclein aggregation in a progressive mouse model of Parkinson's disease. *Brain Res* 956: 156–165, 2002.
40. Nuytemans K, Rademakers R, Theuns J, Pals P, Engelborghs S, Pickut B, de Pooter T, Peeters K, Mattheijssens M, Van den Broeck M, Cras P, De Deyn PP, and van Broeckhoven C. Founder mutation p.R1441C in the leucine-rich repeat kinase 2 gene in Belgian Parkinson's disease patients. *Eur J Hum Genet* 16: 471–479, 2008.
41. Pan T, Kondo S, Le W, and Jankovic J. The role of autophagy-lysosome pathway in neurodegeneration associated with Parkinson's disease. *Brain* 131: 1969–1978, 2008.
42. Plowey ED, Cherra SJ, 3rd, Liu YJ, and Chu CT. Role of autophagy in G2019S-LRRK2-associated neurite shortening in differentiated SH-SY5Y cells. *J Neurochem* 105: 1048–1056, 2008.
43. Rajput A, Dickson DW, Robinson CA, Ross OA, Dachsel JC, Lincoln SJ, Cobb SA, Rajput ML, and Farrer MJ. Parkinsonism, Lrrk2 G2019S, and tau neuropathology. *Neurology* 67: 1506–1508, 2006.
44. Ramirez A, Heimbach A, Grundemann J, Stiller B, Hampshire D, Cid LP, Goebel I, Mubaidin AF, Wriekat AL, Roeper J, Al-Din A, Hillmer AM, Karsak M, Liss B, Woods CG, Behrens MI, and Kubisch C. Hereditary parkinsonism with dementia is caused by mutations in ATP13A2, encoding a lysosomal type 5 P-type ATPase. *Nat Genet* 38: 1184–1191, 2006.
45. Rivera VM, Squillace RM, Miller D, Berk L, Wardwell SD, Ning Y, Pollock R, Narasimhan NI, Iuliucci JD, Wang F, and Clackson T. Ridaforolimus (AP23573; MK-8669), a potent mTOR inhibitor, has broad antitumor activity and can be optimally administered using intermittent dosing regimens. *Mol Cancer Ther* 10: 1059–1071, 2011.
46. Rubinsztein DC. The roles of intracellular protein-degradation pathways in neurodegeneration. *Nature* 443: 780–786, 2006.
47. Saha S, Guillily MD, Ferree A, Lanceta J, Chan D, Ghosh J, Hsu CH, Segal L, Raghavan K, Matsumoto K, Hisamoto N, Kuwahara T, Iwatsubo T, Moore L, Goldstein L, Cookson M, and Wolozin B. LRRK2 modulates vulnerability to mitochondrial dysfunction in *Caenorhabditis elegans*. *J Neurosci* 29: 9210–9218, 2009.
48. Santpere G and Ferrer I. LRRK2 and neurodegeneration. *Acta Neuropathol* 117: 227-46, 2009.
49. Schapira AH. Mitochondrial dysfunction in neurodegenerative diseases. *Neurochem Res* 33: 2502–2509, 2008.
50. Shin N, Jeong H, Kwon J, Heo HY, Kwon JJ, Yun HJ, Kim CH, Han BS, Tong Y, Shen J, Hatano T, Hattori N, Kim KS, Chang S, and Seol W. LRRK2 regulates synaptic vesicle endocytosis. *Exp Cell Res* 314: 2055–2065, 2008.
51. Smith WW, Pei Z, Jiang H, Dawson VL, Dawson TM, and Ross CA. Kinase activity of mutant LRRK2 mediates neuronal toxicity. *Nat Neurosci* 9: 1231–1233, 2006.
52. Squillace RM, Miller D, Cookson M, Wardwell SD, Moran L, Clapham D, Wang F, Clackson T, and Rivera VM. Antitumor activity of ridaforolimus and potential cell-cycle determinants of sensitivity in sarcoma and endometrial cancer models. *Mol Cancer Ther* 10: 1959–1968, 2011.
53. Sultana R and Butterfield DA. Identification of the oxidative stress proteome in the brain. *Free Radic Biol Med* 50: 487–494, 2011.
54. Taylor JP, Mata IF, and Farrer MJ. LRRK2: A common pathway for parkinsonism, pathogenesis and prevention? *Trends Mol Med* 12: 76–82, 2006.
55. Taymans JM and Cookson MR. Mechanisms in dominant parkinsonism: The toxic triangle of LRRK2, alpha-synuclein, and tau. *Bioessays* 32: 227–235, 2010.
56. Ved R, Saha S, Westlund B, Perier C, Burnam L, Sluder A, Hoener M, Rodrigues CM, Alfonso A, Steer C, Liu L, Przedborski S, and Wolozin B. Similar patterns of mitochondrial vulnerability and rescue induced by genetic modification of alpha-synuclein, parkin, and DJ-1 in *Caenorhabditis elegans*. *J Biol Chem* 280: 42655–42668, 2005.
57. West AB, Moore DJ, Biskup S, Bugayenko A, Smith WW, Ross CA, Dawson VL, and Dawson TM. Parkinson's disease-associated mutations in leucine-rich repeat kinase 2 augment kinase activity. *Proc Natl Acad Sci USA* 102: 16842–16847, 2005.
58. West AB, Moore DJ, Choi C, Andrabi SA, Li X, Dikeman D, Biskup S, Zhang Z, Lim KL, Dawson VL, and Dawson TM. Parkinson's disease-associated mutations in LRRK2 link enhanced GTP-binding and kinase activities to neuronal toxicity. *Hum Mol Genet* 16: 223–232, 2007.
59. Wszolek ZK, Tsuboi Y, Ghetti B, Pickering-Brown S, Baba Y, and Cheshire WP. Frontotemporal dementia and parkinsonism linked to chromosome 17 (FTDP-17). *Orphanet J Rare Dis* 1: 30, 2006.
60. Yang Q and Mao Z. Parkinson disease: A role for autophagy? *Neuroscientist* 16: 335–341, 2010.
61. Zimprich A, Biskup S, Leitner P, Lichtner P, Farrer M, Lincoln S, Kachergus J, Hulihan M, Uitti RJ, Calne DB, Stoessl AJ, Pfeiffer RF, Patenge N, Carbajal IC, Vieregge P, Asmus F, Muller-Myhsok B, Dickson DW, Meitinger T, Strom TM, Wszolek ZK, and Gasser T. Mutations in LRRK2 cause autosomal-dominant parkinsonism with pleomorphic pathology. *Neuron* 44: 601–607, 2004.

Address correspondence to:
Prof. D. Allan Butterfield
Department of Chemistry
Center of Membrane Sciences
Sanders-Brown Center on Aging
University of Kentucky
Lexington, KY 40506

E-mail: dabcns@uky.edu

Date of first submission to ARS Central, September 28, 2011; date of final revised submission, January 14, 2012; date of acceptance, January 16, 2012.

Abbreviations Used

HNE = 4-hydroxy-2-nonenal
LB/LN = Lewy bodies/Lewy neuritis
LRRK2 = leucine-rich repeat kinase 2
Non-T = nontransgenic
3NT = 3-nitrotyrosine
PD = Parkinson disease
PTM = post-translational modification
ROS/RNS = reactive oxygen species/reactive nitrogen species
Tau = tau V337M transgenic
WT = wild type